Supplementary Information

Low-resistance p-type ohmic contacts to ultra-thin WSe_2 by using a monolayer dopant

Abhinandan Borah,[*,†] Ankur Nipane,[†] Min Sup Choi,[‡] James Hone,[‡] and James T Teherani[†]

†*Department of Electrical Engineering, Columbia University, New York, NY, USA*

‡*Department of Mechanical Engineering, Columbia University, New York, NY, USA*

E-mail: a.borah@columbia.edu

Comparison of our UV-O_3 method with O_2 plasma oxidation

Table S1: O_2 plasma doping from literature compared to our UV–O_3 doping

	This work	Ref[1]	Ref[2]	Ref[3]	Ref[4]	Ref[5]	Ref[6]
Number of layers	3	8	3–50	6–15	7	2–13	>50
Monolayer dopant	yes	no	no	no	no	no	no
Process temperature ($^{\circ}C$)	Room temp	250	N/A	Room temp	Room temp	N/A	250
$2R_C$ (k$\Omega.\mu$m)	0.6	1	N/A	N/A	4.3	N/A	N/A
Doping density (cm^{-2})	4×10^{13}	8×10^{12}	N/A	N/A	N/A	N/A	N/A
$2R_C$ improvement	300×	100×	N/A	N/A	100×	N/A	N/A
Area-selective doping	yes	no	no	no	no	no	no
Low-R_C at at low-temperature	yes	N/A	N/A	N/A	N/A	N/A	N/A

AFM characterization of 2L WSe_2

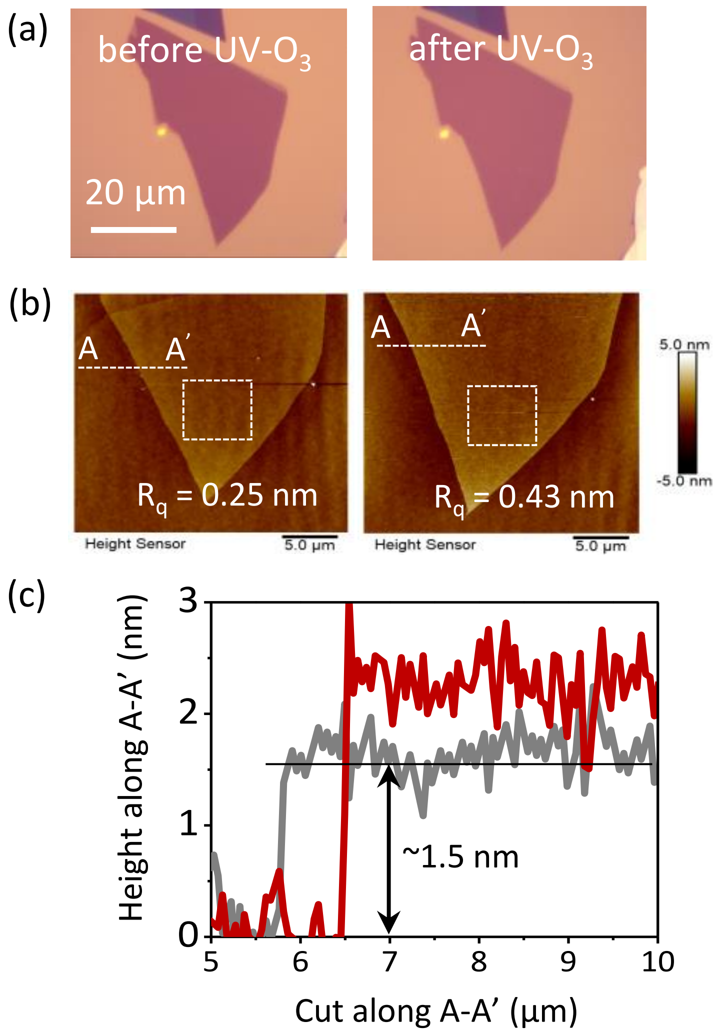

Figure S1: AFM characterization of the bilayer WSe_2 referred in Figure 1 of the main manuscript. (a) Optical microscope image of the flake before (left) and after (right) oxidation. No non-uniformity seen optically after oxidation. (b) AFM topography shows uniform and homogenous oxidation of the entire flake with a slight increase (< 2 Å) in root mean square value of surface roughness, R_q, after oxidation. (c) The height maps along the A-A' cut on the flake before (gray) and after (red) oxidation. Post-oxidation map shows more than 1 nm increase in the height after oxidation due to different bonding configuration of TOS from WSe_2. Further details on this characterization can be found in a different work from our group[7].

AFM characterization of 3L WSe_2

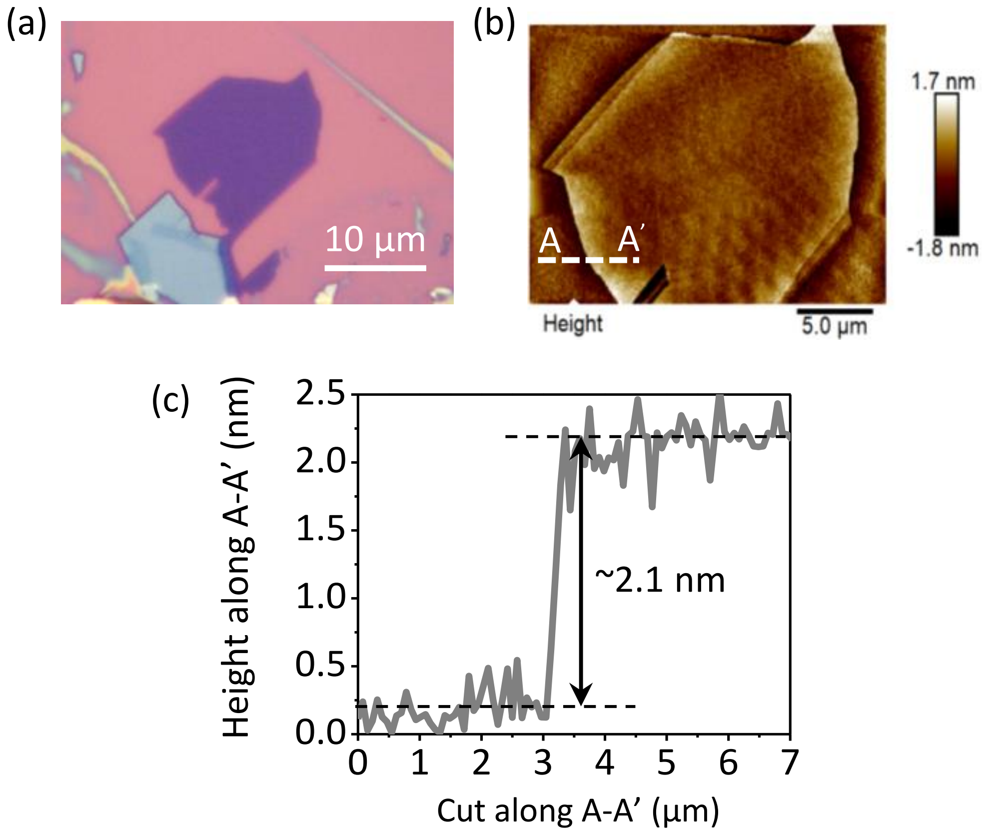

Figure S2: AFM characterization of the WSe_2 used in fabricating the blanket exposure device shown in Figure 2a of main manuscript. (a) The optical microscope image of the flake after exfoliation. (b) Topography of the flake measured before etching into a hall-bar pattern. (c) Height map shows ∼2.1 nm thick flake, which is the approximated thickness for 3L WSe_2[8].

Electrical characterization of multiple devices

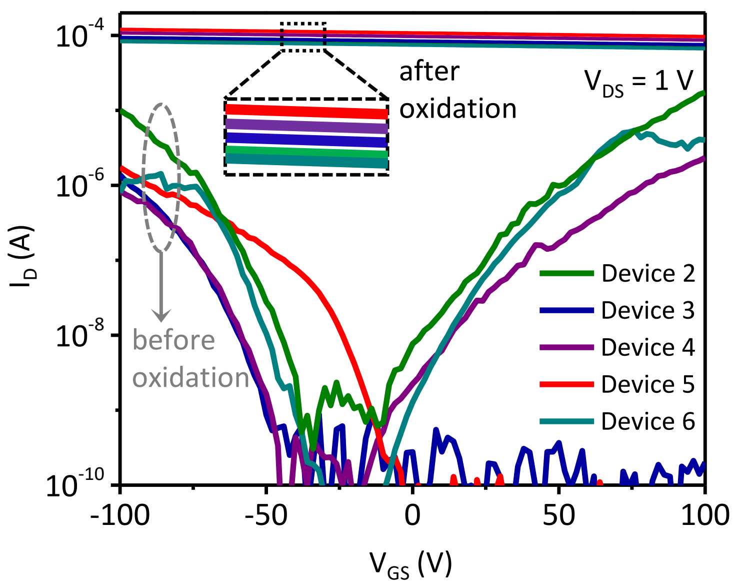

Figure S3: Transfer characteristics of multiple devices before (3L WSe_2) and after oxidation (2L WSe_2 + 1L TOS). Data for device 1 is presented in the Figure 2c in the main manuscript. The channel length and width for all devices are 10 μm and 4μm respectively. The variation in device-characteristics before oxidation is expected for 2D semiconductors and arises during standard lithography steps. Post-oxidation positive shift in threshold voltage and increase in the on-current shows high hole doping. The variation in the current levels post-doping is due to mobility variation (44$-$60 $cm^2/V.s$) among the channels, however the slopes of the transfer curves remain almost same which indicates similar levels of doping in each device ($3{-}4 \times 10^{13}$ cm^{-2}).

Schottky barrier height extraction

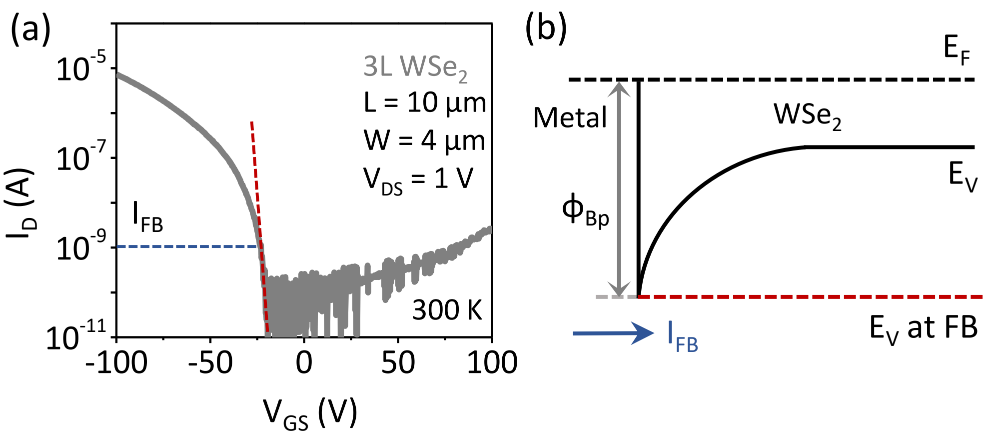

Figure S4: Schottky barrier height extraction for the device shown in Figure 2a in the main manuscript before oxidation (a) Transfer characteristics of the device. The dashed red line is used to find the current at flatband condition, I_{FB}. The V_{GS} at which the transfer characteristics starts deviating from exponential subthreshold behavior is identified as the flatband voltage. The current corresponding to this V_{GS} is the I_{FB} (for this device ~1 nA), which we use to determine the Schottky barrier height before oxidation. (b) The tentative energy band diagram on the source side before doping. Φ_{Bp} is the Schottky barrier height, E_F is the Fermi level and E_V is the valence band edge. The red dashed line shows the valence band edge at flatband condition.

The hole thermionic emission current over a Schottky barrier in a 2D semiconductor is given by[9,10]

$$I_{2D} = W A^*_{2D} T^{3/2} exp(\frac{-q\Phi_{Bp}}{kT})(1 - exp(\frac{qV_D}{kT})) \tag{S1}$$

where W is the width of the semiconductor (4 μm for our device), A^*_{2D} is the modified 2D Richardson's constant, T is the temperature (300 K), Φ_{Bp} is the hole Schottky barrier height, k is the Boltzmann constant, q is a unit charge and V_D is the applied bias (1 V for our measurements). The modified 2D Richardson can be calculated as

$$A^*_{2D} = \frac{q\sqrt{8\pi m^* k^3}}{h^2} \tag{S2}$$

where m^* is the hole effective mass ($0.44\times$mass of an electron for WSe_2)[11] and h is the Placnk's constant. At the flatband condition the tunneling current through the barrier can be assumed zero and any transport is due to the thermionic emission over the barrier. This flatband condition is signified by the point in the transfer characteristics beyond which the current in the subthreshold region starts deviating from exponential behavior[12] (red dashed line in Figure S4). The current at this point is the flatband current, I_{FB}, which is found to be ~1 nA for our device and plugging this I_{FB} for I_{2D} in Eq. (S1), we extract the Schottky barrier height as ~0.35 eV.

References

(1) Pang, C.-S.; Hung, T. Y. T.; Khosravi, A.; Addou, R.; Wang, Q.; Kim, M. J.; Wallace, R. M.; Chen, Z. Atomically Controlled Tunable Doping in High-Performance WSe_2 Devices. *Advanced Electronic Materials* **2020**, *6*, 1901304.

(2) Arnold, A. J.; Schulman, D. S.; Das, S. Thickness Trends of Electron and Hole Conduction and Contact Carrier Injection in Surface Charge Transfer Doped 2D Field Effect Transistors. *ACS Nano* **2020**, *14*, 13557–13568.

(3) Hoffman, A. N.; Stanford, M. G.; Sales, M. G.; Zhang, C.; Ivanov, I. N.; McDonnell, S. J.; Mandrus, D. G.; Rack, P. D. Tuning the electrical properties of WSe_2 via O_2 plasma oxidation: towards lateral homojunctions. *2D Materials* **2019**, *6*, 045024.

(4) Sivan, M.; Li, Y.; Veluri, H.; Zhao, Y.; Tang, B.; Wang, X.; Zamburg, E.; Leong, J. F.; Niu, J. X.; Chand, U.; Thean, A. V.-Y. All WSe_2 1T1R resistive RAM cell for future monolithic 3D embedded memory integration. *Nature Communications* **2019**, *10*, 5201.

(5) Pudasaini, P. R.; Oyedele, A.; Zhang, C.; Stanford, M. G.; Cross, N.; Wong, A. T.; Hoffman, A. N.; Xiao, K.; Duscher, G.; Mandrus, D. G.; Ward, T. Z.; Rack, P. D. High-performance multilayer WSe_2 field-effect transistors with carrier type control. *Nano Research* **2018**, *11*, 722–730.

(6) Kang, W.-M.; Lee, S.; Cho, I.-T.; Park, T. H.; Shin, H.; Hwang, C. S.; Lee, C.; Park, B.-G.; Lee, J.-H. Multi-layer WSe2 field effect transistor with improved carrier-injection contact by using oxygen plasma treatment. *Solid-State Electronics* **2018**, *140*, 2–7.

(7) Nipane, A.; Choi, M. S.; Sebastian, P. J.; Yao, K.; Borah, A.; Deshmukh, P.; Jung, Y.; Kim, B.; Rajendran, A.; Kwock, K. W. C.; Zangiabadi, A.; Menon, V. M.; Schuck, P. J.; Yoo, W. J.; Hone, J.; Teherani, J. T. Damage-Free Atomic Layer Etch of WSe_2: A Platform for Fabricating Clean Two-Dimensional Devices. *ACS Applied Materials & Interfaces* **2020**, 1930–1942.

(8) Fang, H.; Chuang, S.; Chang, T. C.; Takei, K.; Takahashi, T.; Javey, A. High-Performance Single Layered WSe_2 p-FETs with Chemically Doped Contacts. *Nano Letters* **2012**, *12*, 3788–3792.

(9) Kim, C.; Moon, I.; Lee, D.; Choi, M. S.; Ahmed, F.; Nam, S.; Cho, Y.; Shin, H.-J.; Park, S.; Yoo, W. J. Fermi Level Pinning at Electrical Metal Contacts of Monolayer Molybdenum Dichalcogenides. *ACS Nano* **2017**, *11*, 1588–1596.

(10) Ang, Y. S.; Yang, H. Y.; Ang, L. Universal Scaling Laws in Schottky Heterostructures Based on Two-Dimensional Materials. *Physical Review Letters* **2018**, *121*, 056802.

(11) Rasmussen, F. A.; Thygesen, K. S. Computational 2D Materials Database: Electronic Structure of Transition-Metal Dichalcogenides and Oxides. *The Journal of Physical Chemistry C* **2015**, *119*, 13169–13183.

(12) Alharbi, A.; Shahrjerdi, D. Analyzing the Effect of High-k Dielectric-Mediated Doping on Contact Resistance in Top-Gated Monolayer MoS2 Transistors. *IEEE Transactions on Electron Devices* **2018**, *65*, 4084–4092.